STRUCTURAL BIOLOGY

Structural basis for the inhibition of cGAS by nucleosomes

Tomoya Kujirai[1]*, Christian Zierhut[2]*†, Yoshimasa Takizawa[1], Ryan Kim[2], Lumi Negishi[1], Nobuki Uruma[1,3], Seiya Hirai[1,4], Hironori Funabiki[2]‡, Hitoshi Kurumizaka[1,3,4]‡

The cyclic guanosine monophosphate–adenosine monophosphate synthase (cGAS) senses invasion of pathogenic DNA and stimulates inflammatory signaling, autophagy, and apoptosis. Organization of host DNA into nucleosomes was proposed to limit cGAS autoinduction, but the underlying mechanism was unknown. Here, we report the structural basis for this inhibition. In the cryo–electron microscopy structure of the human cGAS–nucleosome core particle (NCP) complex, two cGAS monomers bridge two NCPs by binding the acidic patch of the histone H2A-H2B dimer and nucleosomal DNA. In this configuration, all three known cGAS DNA binding sites, required for cGAS activation, are repurposed or become inaccessible, and cGAS dimerization, another prerequisite for activation, is inhibited. Mutating key residues linking cGAS and the acidic patch alleviates nucleosomal inhibition. This study establishes a structural framework for why cGAS is silenced on chromatinized self-DNA.

The cyclic guanosine monophosphate–adenosine monophosphate (GMP-AMP) synthase (cGAS)–stimulator of interferon genes (STING) pathway senses pathogenic DNA and activates the innate immune system during infections, cancer, and autoimmune diseases (*1*, *2*). DNA sensing is achieved by three distinct DNA binding surfaces on cGAS (sites A, B, and C) (*3*). DNA allosterically activates cGAS to synthesize cyclic GMP-AMP (cGAMP) (*3*–*6*), which then associates with STING (*6*–*11*), promoting autophagy, inflammation, senescence, or apoptosis (*8*, *9*, *12*). A central question is how cGAS avoids activation by self-DNA. Although the nuclear envelope may limit cGAS from accessing chromosomes (*1*, *2*), cGAS signaling is attenuated even when cGAS is forced into the nucleus (*13*). After mitotic nuclear envelope disassembly, cGAS rapidly associates with chromosomes (*14*, *15*), but signaling is largely suppressed (*15*, *16*). Furthermore, although cGAS activation is not observed under normal growth, some cGAS may nonetheless be present within the nucleus (*17*, *18*). cGAS mutations that weaken nuclear tethering of cGAS constitutively activate it without the need for exogenous DNA (*18*), but the structural basis of nuclear tethering and cGAS inhibition remains unclear.

Isolated chromatin (*19*) or reconstituted nucleosomes (*15*) can bind cGAS, but these stimulate cGAMP synthesis less effectively than naked DNA (*15*, *19*, *20*). Furthermore, cGAS has higher affinity for reconstituted nucleosomes than for DNA, and nucleosomes competitively inhibit DNA-dependent cGAS activation (*15*), suggesting that nucleosome binding underlies the inefficient cGAS activation by chromosomes. To monitor nucleosome-dependent suppression under physiological conditions, we used interphase *Xenopus* egg extracts, where exogenously added DNA efficiently assembles into functional chromatin (Fig. 1, A and B) (*21*). When chromatin formation was prevented by depleting histones H3 and H4 from the extract (*21*), exogenously added DNA stimulated cGAMP production after cGAS addition (Fig. 1, A and B). In mock-depleted control extracts, after nucleosome assembly, cGAS activity was severely impaired (Fig. 1, A and B, and fig. S1), indicating that chromatin inhibits cGAS under physiological conditions.

To reveal the mechanism underlying the nucleosome-mediated suppression of cGAS activation, we determined the cryo–electron microscopy (cryo-EM) structure of the complex formed between nucleosome core particles (NCPs) and human cGAS lacking the unstructured N terminus. This construct was chosen because the N terminus induces aggregation and liquid-liquid phase separation, which would interfere with structural analysis (*22*). Native gel electrophoresis confirmed that, similar to nucleosomes with linker DNA, cGAS binds to NCPs with higher affinity than to naked DNA (Fig. 1C). Cryo-EM visualization of these cGAS-NCP complexes showed that most of the NCP-like particles are bridged by cGAS-like particles to form stacks (fig. S2). To obtain higher-resolution EM maps, we used GraFix (*23*). Two major complexes (1 and 2) were isolated and subjected to cryo-EM analysis (fig. S3, A and B). Similar to unfixed samples, most NCP-like particles formed multimers, where cGAS-like particles were seen between NCPs (fig. S3, C and D). Consistent with their gel migration, complex 1 and complex 2 were predominantly composed of two and three NCPs, respectively (fig. S3, C and D). We consider this multimeric configuration to represent the major organization of the cGAS-NCP complex, and we subsequently focused on complex 1, because of its simpler organization (figs. S4 to S6 and table S1). The large majority (86%) of particles in complex 1 that were processed for three-dimensional classification contained

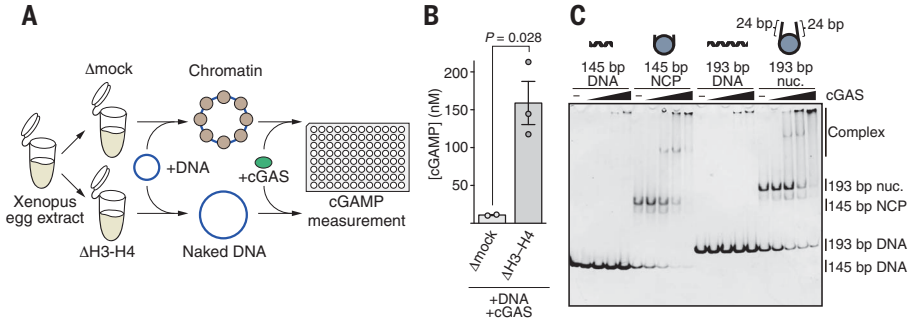

Fig. 1. cGAS-mediated cGAMP synthesis is inhibited by nucleosomes under physiological conditions. (**A**) cGAMP synthesis by cGAS in *Xenopus* egg extracts. Interphase extracts depleted for histones H3 and H4 (ΔH3-H4) or mock-depleted with unspecific antibodies (Δmock) were incubated with exogenously added plasmid DNA and cGAS. After incubation, samples were taken for Western blotting and cGAMP detection by enzyme-linked immunosorbent assay. (**B**) Averages (bars) and SEM (error bars) for the indicated extract types. *P* value derived with unpaired *t* test. (**C**) cGAS-nucleosome binding assay. Increasing amounts of cGAS were mixed with either 145 base-pair (bp) DNA, the nucleosome core particle (NCP) containing 145 bp DNA (no linker DNA), 193 bp DNA, or the nucleosome (nuc.) containing 193 bp DNA (24 bp linker DNA). The indicated species were separated by nondenaturing polyacrylamide gel electrophoresis and visualized with ethidium bromide staining. The result was reproduced in another independent experiment.

[1]Laboratory of Chromatin Structure and Function, Institute for Quantitative Biosciences, The University of Tokyo, 1-1-1 Yayoi, Bunkyo-ku, Tokyo 113-0032, Japan. [2]Laboratory of Chromosome and Cell Biology, The Rockefeller University, New York, NY 10065, USA. [3]Graduate School of Advanced Science and Engineering, Waseda University, 2-2 Wakamatsu-cho, Shinjuku-ku, Tokyo 162-8480, Japan. [4]Department of Biological Sciences, Graduate School of Science, The University of Tokyo, 1-1-1 Yayoi, Bunkyo-ku, Tokyo 113-0032, Japan.
*These authors contributed equally to this work.
†Present address: Division of Cancer Biology, The Institute of Cancer Research, London SW3 6JB, UK.
‡Corresponding author. Email: funabih@rockefeller.edu (H.F.); kurumizaka@iqb.u-tokyo.ac.jp (H.K.)

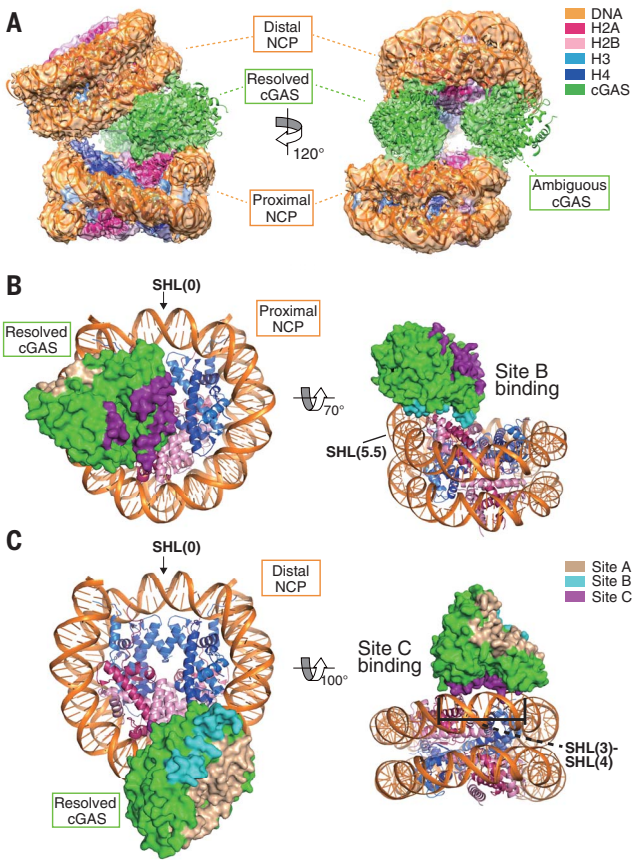

Fig. 2. Cryo-EM structure of the cGAS-nucleosome complex. (**A**) Cryo-EM density of the cGAS-nucleosome complex with fitted structural model. (**B**) cGAS DNA binding site B (cyan) binds the proximal nucleosome through contacts with DNA at SHL5.5 and with the H2A-H2B dimer. (**C**) cGAS DNA binding site C (purple) binds the distal nucleosome at SHL3 and SHL4. DNA binding site A (beige) does not interact with DNA or histones.

two nucleosomes (fig. S4B). Although some of these classes contained one cGAS protomer between two NCPs, suggesting some variability in the possible arrangements, the highest resolution was obtained in the class that contained two cGAS protomers between the two NCPs (fig. S4B).

In the cGAS-NCP complex structure with 3.9-Å resolution (fig. S5), two cGAS monomers bind two NCPs, forming a sandwich-like structure in which the NCPs are intimately associated (Fig. 2A). One cGAS molecule fits well into the cryo-EM map, but the cryo-EM map for the other cGAS molecule is more ambiguous (fig. S6A). A 3.3-Å resolution structure of the resolved cGAS-NCP was generated by a focused refinement after subtraction of the ambiguous cGAS-NCP (figs. S4 and S5). Although resolution of the catalytic pocket is not high enough to assess its local conformation (fig. S5, D and E), it is clear that this cGAS monomer binds to the proximal NCP at the acidic patch on the H2A-H2B histone dimer surface and DNA around superhelical location (SHL) 5.5 (proximal NCP, Fig. 2B); by binding DNA around SHL3 and SHL4 in the other NCP (distal NCP), this cGAS protomer also bridges the two NCPs (Fig. 2, A and C). The ambiguous cGAS monomer may bind to similar NCP surfaces, because cryo-EM densities were observed around nearly symmetric NCP regions (fig. S6C). The ambiguity of this cGAS monomer may reflect its flexibility. Below, we focus our analysis on interactions between the resolved cGAS and the two NCPs.

In previous crystal structures of the cGAS dimer–DNA complex, two cGAS protomers sandwich two DNA fragments, with each cGAS protomer binding one DNA fragment with site A and the other with site B, both of which are essential for cGAS activation (*3*, *4*, *6*, *24*–*27*) (fig. S7). Site C contributes to cGAS activation by promoting DNA-mediated oligomerization (*3*) (fig. S7). Within the cGAS-DNA complex, cGAS dimerization is also important for catalytic activation (*4*). However, direct interaction of the two cGAS protomers in the cGAS-NCP complex is prevented by steric hindrance (fig. S8). Furthermore, the configuration of each cGAS DNA binding site is reorganized in the context of NCP binding in a manner that is incompatible with binding to exogenous DNA.

Although site A is solvent-exposed in the cGAS-NCP complex and does not contact nucleosomal DNA (Fig. 3A, left panel), it is inaccessible to exogenous DNA owing to steric clashes with the proximal NCP (Fig. 3A, right panel). The lack of interactions at site A in the NCP complex is consistent with our previous findings that site A mutations do not affect the affinity of cGAS for mononucleosomes nor cGAS association with mitotic chromosomes (*15*).

Site B is repurposed, with a loop segment binding histones rather than DNA (Fig. 2B). Rather than binding DNA, R236, K254, and R255 of the loop directly bind to the acidic patch of the proximal NCP (Fig. 3B), a hotspot for chromatin interactors (*28*). The side-chain density of cGAS R255 is clearly visible, revealing that R255 interacts with residues E61, D90, and E92 of histone H2A (Fig. 3B), forming a classic arginine anchor such as that found in Kaposi's sarcoma LANA (latency-associated nuclear antigen) peptide (fig. S9). As previously indicated (*18*), this loop is conserved among vertebrate cGAS homologs (fig. S10) but not in the RNA-activated cGAS paralog OAS1 (2′-5′-oligoadenylate synthase 1) (figs. S10 and S11). In addition, an α helix within site B (residues 346 to 355) is located near the DNA around SHL5.5 of the proximal NCP. K347 and K350 within this α helix may interact with the major groove and the backbone of the nucleosomal DNA, respectively (Fig. 3C). The main-chain moieties of several other site B residues, K327, S328, S329, and L354, are located close to R71 of histone H2A and may stabilize the cGAS-NCP interaction (Fig. 3D). Altogether, key residues of site B that are essential for DNA-mediated cGAS activation (*3*, *5*, *25*–*27*) are blocked by the NCP in the cGAS-NCP complex.

cGAS DNA binding site C (fig. S7) binds DNA of the distal NCP in the cGAS-NCP complex (Fig. 2C). Residues 273 to 290 of an α helix within site C are located near nucleosomal DNA around SHL3 (Fig. 3E). In this α helix, the basic residues R281, K282, and K285 may interact with the DNA backbone (Fig. 3E). The KRKR loop (K299, R300, K301, and R302) (*3*) may also interact with nucleosomal DNA around SHL3 (Fig. 3E). K427, K428, and H429, which form the KKH loop (*3*), may interact with nucleosomal DNA around SHL4 (Fig. 3F). In this context, site C cannot access DNA in trans outside of the complex. This potentially suppresses liquid-liquid phase separation–mediated enrichment of cGAS to nucleosome-free DNA within chromatin (*3*, *22*). Gel shift analysis shows that although cGAS mutated at these site C basic residues can bind NCPs to

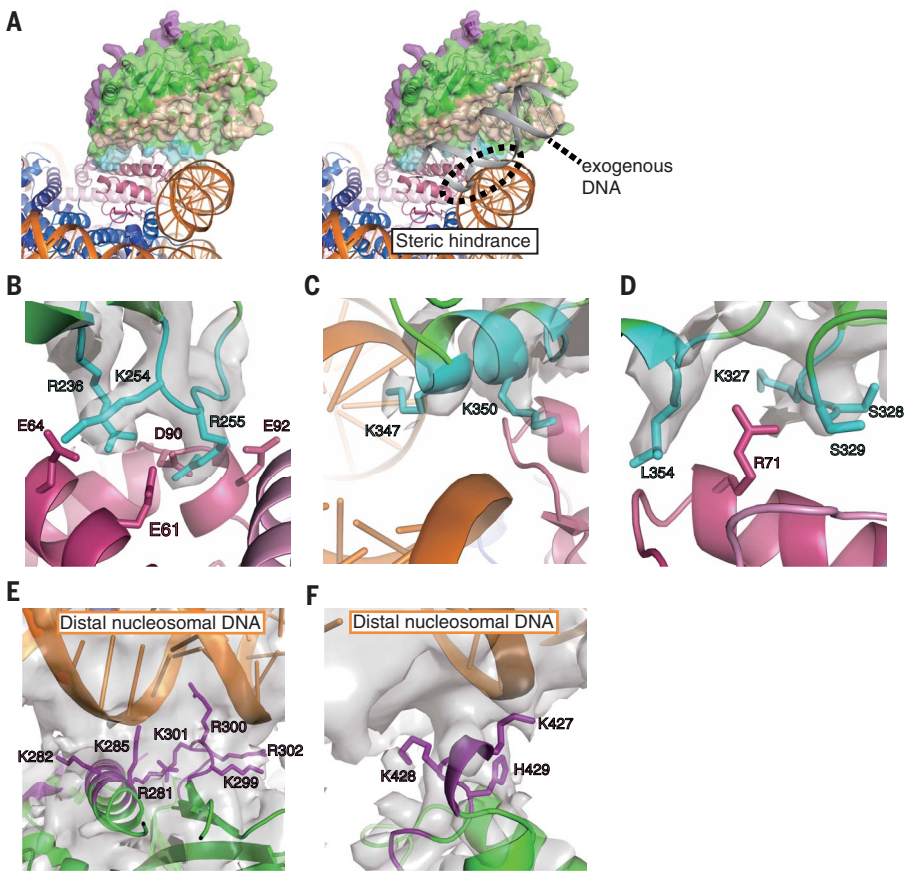

Fig. 3. cGAS-nucleosome interactions. (**A**) Close-up view of cGAS DNA binding site A in the complex (left). The human cGAS-DNA structure [light gray; Protein Data Bank (PDB) ID 6CT9] and the cGAS-nucleosome structure were superimposed by aligning cGAS (right). Binding of exogenous DNA to site A would cause steric clash with nucleosomal DNA. (**B** to **D**) Interactions between the nucleosome and cGAS DNA binding site B. Close-up views of the cGAS residues (B) R236, K254, and R255; (C) K347 and K350; and (D) L354, K327, S328, and S329 are shown. The focused refined EM-density map after subtraction of the ambiguous cGAS-distal nucleosome (see Materials and Methods section of the supplementary materials) was used for representations. Single-letter abbreviations for the amino acid residues are as follows: A, Ala; D, Asp; E, Glu; H, His; K, Lys; L, Leu; R, Arg; and S, Ser. (**E** and **F**) Interactions between the nucleosome and cGAS DNA binding site C. Close-up views of (E) the cGAS α helix region containing R281, K282, and K285 and the KRKR loop containing K299, R300, K301, and R302; and (F) the KKH loop containing K427, K428, and H429 are shown. The EM-density map of the overall structure of the cGAS-nucleosome complex was used for representation. cGAS DNA binding sites are colored as in Fig. 2.

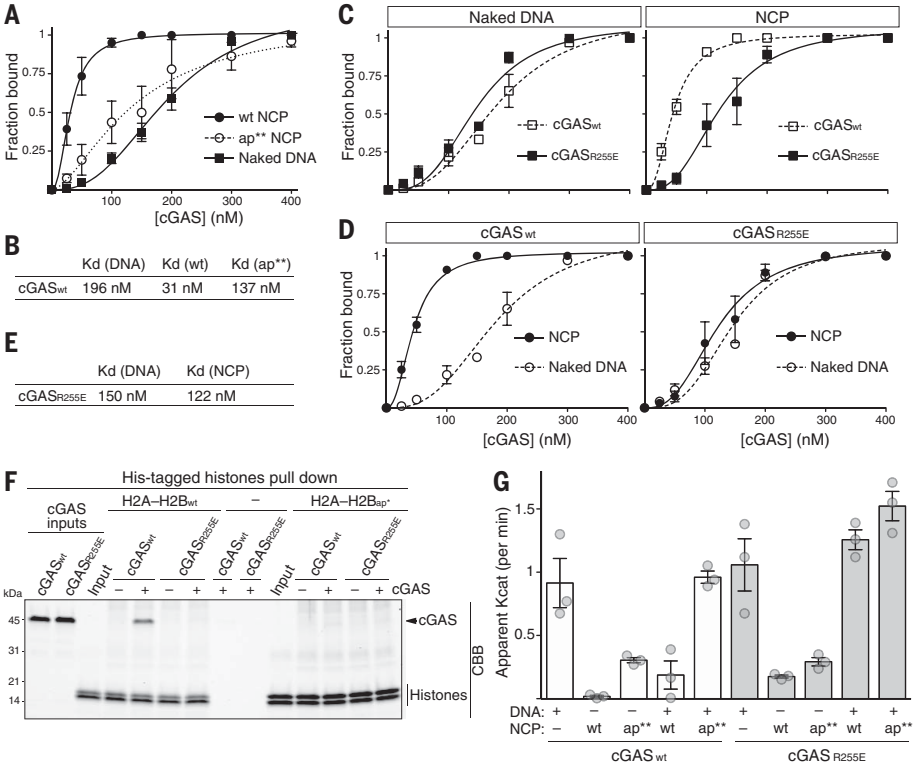

Fig. 4. The acidic patch on the nucleosome and R255 of cGAS are required for high-affinity association between nucleosomes and cGAS and for competitive inhibition of cGAS by nucleosomes. (**A** and **B**) Quantitative gel shift analysis of the binding affinity between cGAS and naked DNA or the indicated nucleosomes (wt, wild type; ap**, acidic patch mutated). See fig. S13A for example gels. Data represent mean and SEM of four independent experiments. 145 bp naked DNA or NCPs containing 145 bp of DNA were used. (**C** to **E**) Quantitative gel shift analysis of the binding affinity between naked DNA or wt nucleosomes and the indicated cGAS. Note that (C) and (D) are different representations of the same experiments. See fig. S13C for example gels. Data represent mean and SEM of three independent experiments. 145 bp naked DNA or NCPs containing 145 bp of DNA were used. (**F**) Analysis of the interaction between cGAS (wt or R255E) and either wt hexahistidine (His_6)–tagged H2A-H2B dimers or acidic patch mutated (ap*) His_6–H2A-H2B dimers. cGAS, histones, and talon beads were mixed, incubated, and collected on a magnet. After washing, bound proteins were separated by gel electrophoresis and visualized with Coomassie brilliant blue (CBB). Equal fractions of inputs and pull-downs were loaded. Results were confirmed in two additional independent experiments. (**G**) Quantifications of catalytic activity of the indicated cGAS version with naked DNA, wt NCPs, or acidic patch mutated (ap**) NCPs in vitro. Averages (bars) and SEM (error bars) of three experiments (dots) are shown. Naked DNA and NCPs were 145 bp and used at 230 nM each.

form complexes with discrete sizes, it cannot form large multimers (fig. S12), suggesting that site C is required for cGAS to generate NCP stacks.

To confirm our interpretations of NCP-dependent suppression of cGAS activity, we focused on site B interactions with the acidic patch of the NCP (Fig. 3B), as site C mutations inactivate human cGAS (*3*). Mutating the acidic patch [ap** H2A: Glu^{56}→Thr (E56T), E61T, E64T, D90S, E91T, and E92T; and ap** H2B: E105T and E113T] abrogated the high-affinity interaction between cGAS and the NCP (Fig. 4, A and B, and fig. S13A). R255 of cGAS site B, which binds the acidic patch (Fig. 3B), is highly conserved in vertebrates but is predicted not to be involved in DNA binding (*18*) (fig. S10). In cells, mutating R255 and the equivalent R241 of mouse cGAS to glutamic acid was reported to weaken the tight nuclear tethering of cGAS (*18*). To test whether R255 is critical for NCP binding, we prepared mutant human cGAS, in which R255 was replaced by glutamic acid ($cGAS_{R255E}$, fig. S13B). Consistent with our structure model, NCP binding of $cGAS_{R255E}$ was decreased, whereas DNA binding was largely unaffected (Fig. 4, B to E, and fig. S13C). Unlike wild-type cGAS that binds NCPs with higher affinity than naked DNA, $cGAS_{R255E}$ did not show such preference (Fig. 4, B to E). Furthermore, although wild-type cGAS bound to H2A-H2B dimers, this interaction was not observed for $cGAS_{R255E}$ (Fig. 4F). Similarly, as we showed previously (*15*), acidic patch mutations in H2A and H2B (ap* H2A: E56A, E61A, E64A, D90A, E91A, and E92A; and ap* H2B: E113A) also interfere with cGAS interaction (Fig. 4F). These data indicate that the interaction between R255 of cGAS and the nucleosome acidic patch is crucial for specific binding of cGAS to nucleosomes.

To test whether this interaction is important for inhibition of DNA-dependent cGAS activation, we monitored how naked DNA, wild-type NCPs, or ap** NCPs stimulate cGAMP production by wild-type cGAS or $cGAS_{R255E}$. In contrast to the almost complete inhibition of cGAMP production by wild-type NCPs with wild-type cGAS, using either $cGAS_{R255E}$ or ap** NCPs increased cGAMP production (Fig. 4G and figs. S14 and S15), supporting the importance of interactions between cGAS and the acidic patch for cGAS inhibition. However, this did not lead to full activation of cGAS (Fig. 4G and fig. S14), likely because of the conformation of nucleosomal DNA, which may not be optimal for cGAS activation. On naked DNA, cGAS makes many contacts with the backbone of more than a full turn of DNA, which is in a straight conformation (*3*, *4*, *24*–*27*) (fig. S7). In contrast, the curvature of DNA wrapped around the histone octamer may interfere with the structural changes in cGAS required for full catalytic activity (example shown in fig. S16).

The significance of the cGAS–acidic patch interactions for cGAS inhibition was better illustrated when competitive inhibition of naked DNA–stimulated cGAMP production was assessed (Fig. 4G, combinations of DNA and wild-type or ap** NCPs). Whereas wild-type NCPs were able to competitively inhibit wild-type cGAS activation by an equal amount of naked DNA, ap** NCPs lost this inhibitory activity (Fig. 4G, left). In contrast, $cGAS_{R255E}$ was refractory to inhibition by even wild-type NCPs (Fig. 4G, right). Moreover, whereas wild-type cGAS is suppressed by NCPs with or without the linker DNA, $cGAS_{R255E}$ is activated by NCPs with linker DNA but not by NCPs without linker DNA (fig. S17). These findings predict that $cGAS_{R255E}$, which cannot be competitively inhibited by NCPs, is activated by nucleosome-free segments of genomic DNA in cells. Indeed, in HeLa cells expressing $cGAS_{R255E}$, high basal levels of cGAMP have been observed (*18*). Altogether, these structural, biochemical, and cellular analyses support the importance of the interaction between cGAS site B and the nucleosome acidic patch in competitive inhibition of DNA-dependent cGAS activation.

The competitive inhibition by nucleosomes can explain how stimulation of cGAS by chromosomal self-DNA can be prevented, despite the presence of nucleosome-free regions. Our analysis indicates that NCPs can competitively inhibit cGAS activation by at least four mechanisms (fig. S18). First, DNA binding at site A is prevented by steric clashes with the proximal NCP. Second, site B is occupied by the acidic patch of the proximal NCP and therefore is inaccessible to exogenous DNA. Third, cGAS dimerization is prevented by steric clashes with the proximal NCP. Fourth, the formation of tandem cGAS-NCP chains via sites B and C prevents cGAS-DNA oligomerization, which is required for full activation (*3*, *4*). However, the fourth mechanism may be species specific, because several site C basic residues that are predicted to contact nucleosomal DNA, such as those in the KRKR and KKH loops, are not highly conserved (*3*) (fig. S10). As human and mouse cGAS exhibit different enzymatic, DNA-length sensitivity, and phase-separation characteristics (*3*, *22*), chromatin inhibition of cGAS may also be modified species-specifically. It is likely that diverse mechanisms, such as the expression of H2A variants that lack the acidic patch, regulate the nucleosome-dependent suppression of cGAS.

REFERENCES AND NOTES

1. A. Ablasser, Z. J. Chen, *Science* **363**, eaat8657 (2019).
2. M. Motwani, S. Pesiridis, K. A. Fitzgerald, *Nat. Rev. Genet.* **20**, 657–674 (2019).
3. W. Xie *et al.*, *Proc. Natl. Acad. Sci. U.S.A.* **116**, 11946–11955 (2019).
4. X. Li *et al.*, *Immunity* **39**, 1019–1031 (2013).
5. R. M. Hooy, J. Sohn, *eLife* **7**, e39984 (2018).
6. P. Gao *et al.*, *Cell* **153**, 1094–1107 (2013).
7. H. Ishikawa, G. N. Barber, *Nature* **455**, 674–678 (2008).
8. L. Sun, J. Wu, F. Du, X. Chen, Z. J. Chen, *Science* **339**, 786–791 (2013).
9. J. Wu *et al.*, *Science* **339**, 826–830 (2013).
10. A. Ablasser *et al.*, *Nature* **498**, 380–384 (2013).
11. K. Kato, H. Omura, R. Ishitani, O. Nureki, *Annu. Rev. Biochem.* **86**, 541–566 (2017).
12. H. Ishikawa, Z. Ma, G. N. Barber, *Nature* **461**, 788–792 (2009).
13. M. Gentili *et al.*, *Cell Rep.* **26**, 2377–2393.e13 (2019).
14. H. Yang, H. Wang, J. Ren, Q. Chen, Z. J. Chen, *Proc. Natl. Acad. Sci. U.S.A.* **114**, E4612–E4620 (2017).
15. C. Zierhut *et al.*, *Cell* **178**, 302–315.e23 (2019).
16. L. Zhong *et al.*, *Cell Discov.* **6**, 26 (2020).
17. H. Jiang *et al.*, *EMBO J.* **38**, e102718 (2019).
18. H. E. Volkman, S. Cambier, E. E. Gray, D. B. Stetson, *eLife* **8**, e47491 (2019).
19. K. J. Mackenzie *et al.*, *Nature* **548**, 461–465 (2017).
20. X. Lahaye *et al.*, *Cell* **175**, 488–501.e22 (2018).
21. C. Zierhut, C. Jenness, H. Kimura, H. Funabiki, *Nat. Struct. Mol. Biol.* **21**, 617–625 (2014).
22. M. Du, Z. J. Chen, *Science* **361**, 704–709 (2018).
23. B. Kastner *et al.*, *Nat. Methods* **5**, 53–55 (2008).
24. F. Civril *et al.*, *Nature* **498**, 332–337 (2013).
25. X. Zhang *et al.*, *Cell Rep.* **6**, 421–430 (2014).
26. L. Andreeva *et al.*, *Nature* **549**, 394–398 (2017).
27. W. Zhou *et al.*, *Cell* **174**, 300–311.e11 (2018).
28. A. A. Kalashnikova, M. E. Porter-Goff, U. M. Muthurajan, K. Luger, J. C. Hansen, *J. R. Soc. Interface* **10**, 20121022 (2013).

ACKNOWLEDGMENTS

We thank Y. Iikura and J. Kato (University of Tokyo) for their assistance and Y. Arimura for helpful discussions and comments on the manuscript. We also thank M. Kikkawa for cryo-EM data collection. **Funding:** This work was supported in part by JSPS KAKENHI grants JP17H01408 (to H.K.), JP18H05534 (to H.K.), JP19K06522 (to Y.T.), and JP20K15711 (to T.K.); JST CREST grant JPMJCR16G1 (to T.K. and H.K.); the Platform Project for Supporting Drug Discovery and Life Science Research (BINDS) from AMED under grants JP20am0101076 (to H.K.) and JP20am0101115j0004 (to M. Kikkawa); JST ERATO grant JPMJER1901 (to H.K.); and National Institutes of Health grant R35GM132111 (to H.F.). **Author contributions:** C.Z., R.K., T.K., and N.U. purified cGAS proteins. T.K. and S.H. prepared the cGAS-nucleosome complex. C.Z., R.K., T.K., S.H., and L.N. performed biochemical analyses. T.K. and Y.T. performed the cryo-EM analysis. T.K., C.Z., H.F., and H.K. conceived of and designed the work. T.K., C.Z., R.K., H.F., and H.K. wrote the paper. H.F. and H.K. guided and supervised all of the work. All of the authors discussed the results and commented on the manuscript. **Competing interests:** The authors declare no competing interests. H.F. is affiliated with the Graduate School of Medical Sciences, Weill Cornell Medicine, and the Cell Biology Program of the Sloan Kettering Institute. **Data and materials availability:** The cryo-EM reconstructions and atomic model of the cGAS-nucleosome complex have been deposited in the Electron Microscopy Data Bank and the Protein Data Bank under accession code EMD-30267 and PDB ID 7C0M. All data and materials are available from the corresponding authors upon request.

SUPPLEMENTARY MATERIALS

science.sciencemag.org/content/370/6515/455/suppl/DC1
Materials and Methods
Figs. S1 to S18
Table S1
References (*29*–*47*)
MDAR Reproducibility Checklist

View/request a protocol for this paper from *Bio-protocol*.

27 May 2020; accepted 28 August 2020
Published online 10 September 2020
10.1126/science.abd0237

Science

Structural basis for the inhibition of cGAS by nucleosomes

Tomoya Kujirai, Christian Zierhut, Yoshimasa Takizawa, Ryan Kim, Lumi Negishi, Nobuki Uruma, Seiya Hirai, Hironori Funabiki and Hitoshi Kurumizaka

Science **370** (6515), 455-458.
DOI: 10.1126/science.abd0237originally published online September 10, 2020

Saving a host cell from itself

A fundamental mammalian defense mechanism against pathogens and damaged cellular DNA is to recognize DNA fragments in the cytosol and trigger an inflammatory response. The cyclic guanosine monophosphate–adenosine monophosphate synthase (cGAS) that recognizes cytosolic DNA is also found in the nucleus, but here its activity is suppressed by tethering to chromatin. Two papers now report cryo–electron microscopy structures of cGAS bound to the nucleosome core particle (NCP). Kujirai *et al.* observed a structure with two cGAS molecules bridging two NCPs, whereas Boyer *et al.* observed cGAS bound to a single nucleosome. Together, these structures show how cGAS is prevented from autoreactivity toward host DNA.

Science, this issue p. 455, p. 450